



Article

Turbulent Energy and Carbon Fluxes in an Andean Montane Forest—Energy Balance and Heat Storage

Charuta Murkute ^{1,*}, Mostafa Sayeed ¹, Franz Pucha-Cofrep ^{1,2}, Galo Carrillo-Rojas ³, Jürgen Homeier ⁴, Oliver Limberger ⁵, Andreas Fries ², Jörg Bendix ⁵ and Katja Trachte ¹

- Department of Atmospheric Processes, Brandenburg University of Technology Cottbus-Senftenberg, Burger Chaussee 2, 03046 Cottbus, Germany; sayeemos@b-tu.de (M.S.); fapucha@utpl.edu.ec (F.P.-C.); trachte@b-tu.de (K.T.)
- ² Hydrology and Climatology Working Group, Departamento de Ingeniería Civil, Universidad Técnica Particular de Loja, San Cayetano Alto, C. París, Loja 110107, Ecuador; aefries@utpl.edu.ec
- Departamento de Recursos Hídricos y Ciencias Ambientales, Facultad de Ciencias Químicas, Universidad de Cuenca, Av. Víctor Manuel Albornoz y los Cerezos, Cuenca 010107, Ecuador; galo.carrillo@ucuenca.edu.ec
- ⁴ Faculty of Resource Management, HAWK University of Applied Sciences and Arts, Daimlerstraße 2, 37075 Göttingen, Germany; jhomeie@gwdg.de
- Laboratory for Climatology and Remote Sensing, Department of Geography, University of Marburg, Deutschhausstrasse 12, 35032 Marburg, Germany; oliver.limberger@geo.uni-marburg.de (O.L.); bendix@staff.uni-marburg.de (J.B.)
- * Correspondence: murkute@b-tu.de

Abstract: High mountain rainforests are vital in the global energy and carbon cycle. Understanding the exchange of energy and carbon plays an important role in reflecting responses to climate change. In this study, an eddy covariance (EC) measurement system installed in the high Andean Mountains of southern Ecuador was used. As EC measurements are affected by heterogeneous topography and the vegetation height, the main objective was to estimate the effect of the sloped terrain and the forest on the turbulent energy and carbon fluxes considering the energy balance closure (EBC) and the heat storage. The results showed that the performance of the EBC was generally good and estimated it to be 79.5%. This could be improved when the heat storage effect was considered. Based on the variability of the residuals in the diel, modifications in the imbalances were highlighted. Particularly, during daytime, the residuals were largest (56.9 W/m² on average), with a clear overestimation. At nighttime, mean imbalances were rather weak (6.5 W/m²) and mostly positive while strongest underestimations developed in the transition period to morning hours (down to -100 W/m²). With respect to the Monin-Obukhov stability parameter ((z - d)/L) and the friction velocity (u^*) , it was revealed that the largest overestimations evolved in weak unstable and very stable conditions associated with large u* values. In contrast, underestimation was related to very unstable conditions. The estimated carbon fluxes were independently modelled with a non-linear regression using a light-response relationship and reached a good performance value ($R^2 = 0.51$). All fluxes were additionally examined in the annual course to estimate whether both the energy and carbon fluxes resembled the microclimatological conditions of the study site. This unique study demonstrated that EC measurements provide valuable insights into land-surface-atmosphere interactions and contribute to our understanding of energy and carbon exchanges. Moreover, the flux data provide an important basis to validate coupled atmosphere ecosystem models.

Keywords: energy balance closure; heat storage; carbon fluxes; eddy covariance; Andes Mountains



Citation: Murkute, C.; Sayeed, M.; Pucha-Cofrep, F.; Carrillo-Rojas, G.; Homeier, J.; Limberger, O.; Fries, A.; Bendix, J.; Trachte, K. Turbulent Energy and Carbon Fluxes in an Andean Montane Forest—Energy Balance and Heat Storage. *Forests* 2024, 15, 1828. https://doi.org/ 10.3390/f15101828

Received: 3 September 2024 Revised: 13 October 2024 Accepted: 17 October 2024 Published: 20 October 2024



Copyright: © 2024 by the authors. Licensee MDPI, Basel, Switzerland. This article is an open access article distributed under the terms and conditions of the Creative Commons Attribution (CC BY) license (https://creativecommons.org/licenses/by/4.0/).

1. Introduction

Tropical forests play a vital role in the global carbon cycle and serve as substantial carbon sinks [1-3]. Through their dynamic exchanges of energy, water, and carbon, they shape climate patterns not only regionally but also on a global scale [1-4]. However,

Forests **2024**, 15, 1828 2 of 22

ongoing climate change significantly impacts these land-surface—atmosphere exchange processes. Rising temperatures increase the evaporative demand, which feeds back to photosynthetic activities, as indicated by the net ecosystem exchange (NEE) [5,6]. Previous research by [1,5,7–11] has focused on the carbon annual budgets of tropical rainforests. While these studies provided valuable insights into carbon fluxes, they did not specifically address the complexities introduced by heterogeneous terrain. Their findings emphasize the need for dedicated studies that consider the influence of topography on ecosystem carbon dynamics. The tropical mountain rainforest in the Andes Mountains of southern Ecuador represents a unique and biodiverse ecosystem that has received comparatively little attention regarding exchange processes at the ecosystem atmosphere interface although they are critical for global carbon storage [12]. As described by previous studies, the area is highly endangered by both deforestation [13,14] as well as climate change [15], which impact the exchange of energy, water, and carbon. Thus, knowledge on land-surface–atmosphere interactions encompassing NEE and the surface energy balance (SEB) play an important role in understanding modifications due to global changes.

A commonly used and worldwide accepted approach to directly observe atmospheric carbon and water fluxes is the eddy covariance (EC) measurement technique [16,17]. EC is based on the high-frequency (10-20 Hz) measurements of the vertical wind speed and CO₂/H₂O concentrations above plant canopies (turbulent eddy flux) coupled with measurements of CO₂ storage below the measurement point using slow-response infrared gas analyzers [14]. Applying this technique requires extensive quality checks to ensure the accuracy of the measurements across different surfaces [18]. At the same time, certain conditions such as homogeneous and flat surfaces facilitate the estimation and quantification of the fluxes [16,19]. In order to guarantee the quality of the data, quality assessment and control is mandatory, especially in non-ideal environments such as the mountainous landscape of the Andes. One of the primary challenges associated with EC measurements in complex terrains is the occurrence of stable atmospheric conditions, particularly at night during nocturnal boundary layer (NBL) development. The atmosphere can evolve a thermally stable stratification, which strongly affects turbulent exchanges and a modified turbulent kinetic energy (TKE) [20,21]. This may lead to an accumulation of CO₂ near the surface, causing an underestimation of nighttime ecosystem respiration as a result of a reduced or intermittent TKE [13,14]. In contrast, a decoupling between the NBL and the air masses aloft can induce an overestimation of quantities of flux concertation due to a break-up of the NBL. The result is an energy imbalance as reported by various studies [22-24]. Additionally, due to the sloped surfaces, downslope flows evolve during nighttime until the early morning hours, which tend to enhance carbon uptake [25]. A well-reported problem in complex terrain is the vertical and horizontal advection [26–30]. Ref. [28] showed that during nighttime, due to drainage flows, positive vertical advection fluxes occur while, during daylight periods, vertical flux divergence is associated with horizontal advection. However, the advection fluxes are also complex when it comes to detection [26] and site specific [17].

Further, in tropical rainforests, the often dense canopy structure significantly limits the amount of solar radiation that reaches the forest surface. Consequences of the reduction in ground-level radiation can include a modified SEB being reflected in the energy balance closure (EBC), which is a critical validation step for EC measurements. Again, advection can contribute to the non-closure of the EBC as it enhances the water fluxes, especially in dense canopies [30]. As shown by [31,32], an EBC in an acceptable range is also relevant in the interpretation of the atmospheric H₂O and CO₂ fluxes. However, uncertainties in association to EBC frequently occur. Refs. [20,23] showed that in EC measurements over complex terrain, EBC residuals can reach up to 35%. Additionally, the footprint area of the fluxes can become more variable due to the heterogeneous surface characteristics inducing upslope and downslope flows in the diurnal cycle, which is frequently evolving [33], especially in our study site [13,14]. Further, heat, water vapor, and carbon can accumulate below the level of flux measurements by EC, and this storage tends to be larger in tall

Forests 2024, 15, 1828 3 of 22

canopies as in forest ecosystems. Refs. [34,35] investigated the heat storage effect in midlatitude forest ecosystems and its effect on the EBC. They found a total heat storage varying between -35 and +45 W/m². Not accounting for changes to the storage in the total flux, estimates can create biases in land surface modeling. Ref. [36] showed that biases in sensible and latent fluxes are related to the inability to represent heat storage in vegetation biomass using the Community Land Model, version 5. Ref. [37] also reported on the improvement of the modeling results under the consideration of the heat storage effect of forest ecosystems. Thus, the estimation of uncertainties in EC measurements is crucial and needs careful consideration as these uncertainties are also relevant for coupled atmosphere ecosystem modeling.

However, several studies over the past decade have also successfully utilized EC measurements in complex terrain or non-ideal conditions [32,38,39]. For the European alpine region, the authors of [40] have employed these techniques to manage turbulent advection and account for sloping terrain effects. While these corrections and approaches can help reduce uncertainties in the measurements, these studies also highlight that achieving an accurate and closed energy balance in complex terrain remains a significant challenge for the EC method. Refs. [3,27,41,42], amongst others, have specifically tackled the challenges posed by complex terrain in tropical ecosystems. Refs. [27,41] observed the dependence of u* on the daytime EBC and demonstrated that the EBC was highly related to the thermodynamic stability of the lower atmosphere. In dry tropical forests, ref. [40] successfully used EC measurements in which, based on the TKE, the authors used dimensionless turbulence filters and corrected radiation measurements to address these challenges.

In order to get a better understanding of the energy and carbon exchange in tropical mountain rainforest ecosystems and the response to recent and future climate changes reflected in coupled atmosphere ecosystem modeling, observations are highly needed. Therefore, the main objective of this paper is the analysis of the influence of the terrain complexity and vegetation height on the turbulent exchange of momentum, energy, and carbon using EC measurements above a tropical forest canopy. The aims are to (i) analyze the wind field to assess the advection and turbulent activities, (ii) examine the EBC to estimate the quality of the EC measurements and quantify the imbalance of the heat fluxes and the storage effect of the forest vegetation, and (iii) explore the quality of the carbon fluxes by analyzing the NEE in the diurnal cycle. The accuracy of the measured energy and carbon fluxes is highly important for a subsequent partitioning of the NEE.

2. Data and Methods

2.1. Study Site

The study site is nestled within the tropical montane forest of the Reserva Biológica San Francisco (RBSF), situated on a north-facing slope within the Cordillera Real of the Andes in southern Ecuador, the forest type has been described as evergreen lower montane forest [43]. From a permanent one ha forest plot directly adjacent to the eddy covariance station, we have the following information on forest structure and tree species composition. The species-rich forest contains 1030 stems (with dbh \geq 10 cm) of 88 different tree species per hectare. Trees reach maximum heights of 20 m and, diameters of 75 cm. Most common tree species are Alzatea verticillata (Alzateaceae, 121 stems), Hieronyma fendleri (Phyllanthaceae, 104), Graffenrieda emarginata (Melastomataceae, 73), and the most common tree families are Lauraceae (227 stems), Melastomataceae (125), and Alzateaceae (121). Aboveground tree biomass was estimated to be 175.8 Mg ha^{-1} using the formula of [44]. The climate is dominated by the persistent easterly trade winds [45]. Throughout the study period from 2020 to 2022, the mean annual temperature was recorded at 15.4 °C, with an average annual precipitation of 1854 mm. The soil in this part of the forest has been characterized as humic cambisol, which is covered by a raw humus layer of up to 35 cm thickness [46,47].

Forests **2024**, 15, 1828 4 of 22

2.2. Instrumentation

The eddy flux tower is located at 3.9737° S/79.0751° W at an altitude of 1984 asl (Figure 1). It is equipped with an open-path infrared gas analyzer and 3-D sonic anemometer (IRGASON, Campbell Sci., Logan, UT, USA) to measure H_2O/CO_2 fluxes at a frequency of 10 Hz. The EC system has been installed at a height level of 23 m, with mean canopy height of 14 m. Additional meteorological sensors have been installed over the canopy to measure the radiation components—short-wave incoming (Swin), short-wave outgoing (Swout), longwave incoming (Lwin), and long-wave outgoing (Lwout)—using a net radiometer (NR01, Hukseflux, Campbell Sci., Logan, UT, USA), photosynthetic active radiation (PAR) (SKP215, Skye Instruments, Llandrindod Wells, UK), air temperature (Ta), and relative humidity (RH, VAISALA HMP115, Helsinki, Finland). Precipitation is measured using a tipping bucket rain gauge. To obtain soil conditions, a TDR soil water sensor (CS655, Campbell Scientific, Logan, UT, USA) at a depth of 20 cm has been installed, and this measures both soil moisture content (SWC) as well as soil temperature (Ts). A self-calibrating heat flux plate (HFP01-SC, Hukseflux, Campbell Scientific, Logan, UT, USA) is used to measure the soil heat flux (G). All variables were sampled and averaged to half-hourly intervals using the CR6 data logger (Campbell Scientific). To estimate the temperature and humidity profile below the canopy, Hobologgers (MX2301A, LI-COR, Nebraska, NE, USA) were installed at 1 m, 7 m, 12.5 m, and 16 m. The time period considered for the study was from January 2020 to December 2022. The PAR sensor was available for the time period March–December 2022 and Ta/RH profiles from October to December 2022.

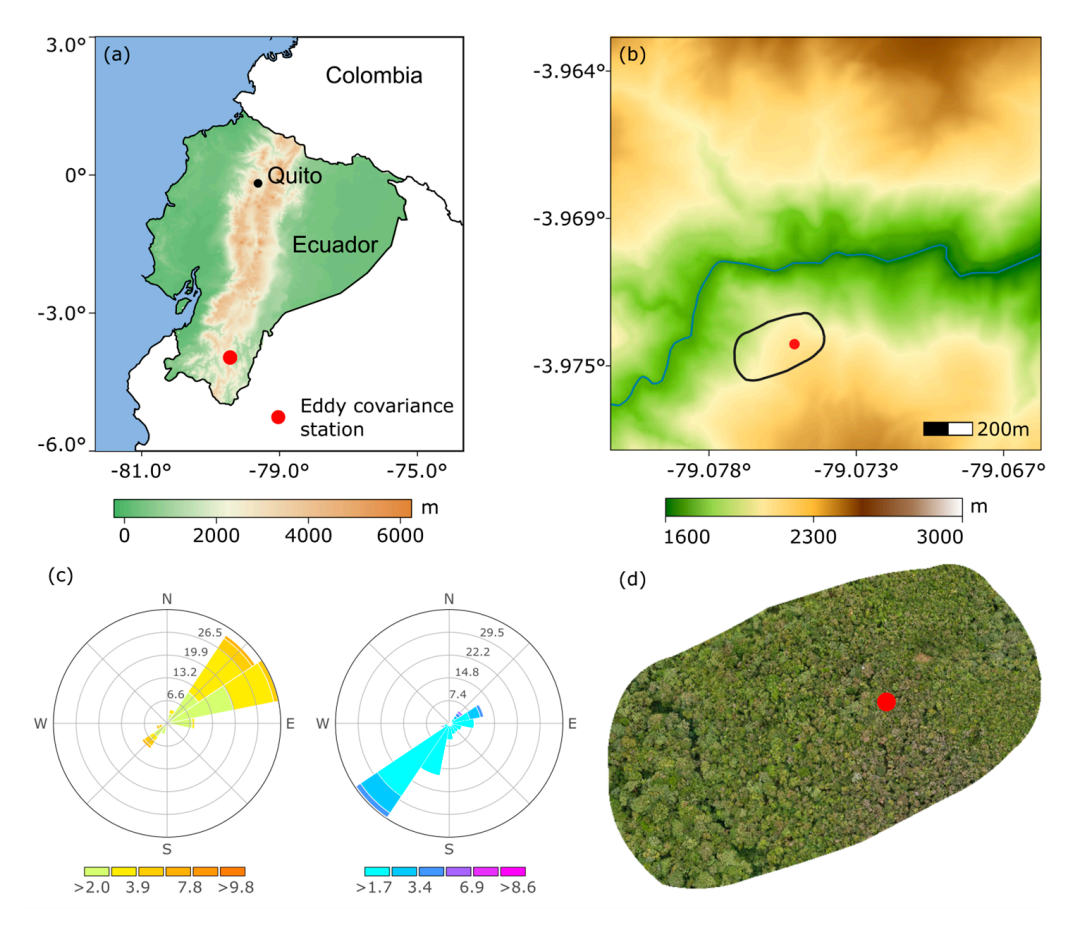


Figure 1. Study area and geographical location of the eddy covariance station. (a) Map of Ecuador, (b) location of the study site including drone image domain, (c) wind rose (m/s) for daytime and nighttime hours, and (d) drone image of the site.

Forests **2024**, 15, 1828 5 of 22

2.3. EC Raw Data Processing

The 10 Hz raw data were processed using EddyPro version 7.0.9 (https://www.licor. com/env/products/eddy_covariance/eddypro, accessed on 11 October 2023). In order to reduce uncertainties in the data and guarantee data quality, various techniques were used. Half-hourly averaged values of the biometeorological variables, which were measured with a lower time resolution (30 min) than EC, were used as an additional input for the EddyPro Software (version 7.0.9) package to obtain better estimates of the fluxes. These variables were measured with a lower time resolution than EC. The full output of EddyPro contained time-synchronized fluxes. Random uncertainties arising out of the flux sampling error were computed following [48]. Other techniques such as despiking [49] and block averaged detrending were applied to the data as well. Low-pass corrections [50] were applied to compensate for the loss of fluxes towards the low- and high-frequency ranges of the cross-spectrum, respectively. Such losses can arise out of inefficient filtering and/or time averaging [51]. WPL corrections accounted for density fluctuations using the classic formulation of [52], ensuring that the effects of water vapor and temperature fluctuations on CO₂ flux were corrected. In addition, coordinate rotation was performed using the planar-fit method with wind sector divided into 30° [53]. The footprint of the EC tower was calculated according to [54].

2.4. Processing the Half Hourly Data

The initial processing of the half-hourly interval data produced by EddyPro was subjected to rigorous quality control procedures to ensure the accuracy and reliability of the dataset. Instrumentation failures and malfunction frequently occur at our study site. Because these low-quality data are often not captured by purely statistical methods, we followed [22] and conducted a visually inspection in the first instance. Afterwards, the following methodologies were used for data filtering and cleaning. The primary step in the data quality control process involved spike detection using the Median Absolute Deviation (MAD) method [18]. This robust statistical technique identifies outliers by calculating the median of the absolute deviations from the dataset's median, providing a measure resistant to extreme values. Subsequent to spike detection, a filtering criterion based on the mean \pm 2 standard deviations (SDs) was employed [15]. To further improve the quality of our data, we carefully considered the impact of precipitation events, which significantly influence the fluxes at our study site. Specifically, we discarded data collected during precipitation events, as well as data from periods immediately preceding and following these events.

2.4.1. Energy Flux Data

We carefully separated the data based on nighttime, transition times, and daytime periods. We tested the impact of turbulences on energy fluxes by applying u^* filtering as suggested by [27,32]. The authors applied this filter for nighttime data where values below a threshold of $u^* > 0.23$ were discarded; due to stable conditions, vertical transport was weak, and thus, energy fluxes were underestimated. We also removed high turbulence values, which discarded unrealistic high positive energy flux values, which occurred due to large eddies evolving in down-valley winds. For the daytime period when strong mixing led to high turbulent periods with $0.5 > u^* > 1$, negative or close to zero values were discarded for both LE and H. Such values were often observed during peak noon period, usually considered with high turbulence, except the values impacted due to precipitation event. Similarly, during transition periods where u^* was fluctuating between stable and unstable conditions, such ambiguous data periods were mostly discarded, since such extreme values were likely artifacts of turbulent conditions during the transition from stable to unstable periods. Implementing these measures, we aimed to refine our dataset and improve the reliability of the EBC analysis.

Forests **2024**, 15, 1828 6 of 22

2.4.2. NEE Data Filtering

Standard procedure was applied, including u* filtering to exclude low-frequency data obtained during stable conditions. The u* threshold was determined using the moving point technique [55], with a u* threshold of 0.23 m/s. Nighttime negative values of NEE were also discarded.

After applying the filtering processes, including the consideration of u* values and other procedures outlined in Sections 2.4, 2.4.1 and 2.4.2, as well as accounting for contamination from precipitation in flux measurements, the remaining percentages of NEE, H, and LE are summarized in Table 1. Notably, during nighttime hours, very little data remained after applying the u* filtering described [39].

Table 1. Remaining data availability in percentages after filtering. The data were divided into day (11:00–14:00), night (20:00–6:00), and transition (07:00–10:00 and 15:00–19:00) data.

| Filtering | Time | NEE | Н | LE |
|-------------------------|------------|-----|-----|-----|
| Precipitation | Day | 75% | 73% | 73% |
| | Transition | 82% | 73% | 84% |
| | Night | 85% | 85% | 87% |
| All filtering procedure | Day | 54% | 60% | 60% |
| | Transition | 52% | 58% | 58% |
| | Night | 21% | 21% | 21% |

2.5. Correction for Global Radiation

Since the NR01 had been installed over a sloped surface above canopy and, thus, not mounted, perpendicular corrections had to be applied to short-wave incoming radiation (Swin) as the measurements were dependent on the slope and aspect of the surface [40,51]. The model and methodologies presented by [56,57] were thus used to correct the measurements at the sloping site. The procedure requires calculations of the solar zenith angle (θz) and the angle between the horizontal to the inclined surface and the direction of the sun (ψ^2 ; all angles are expressed in radians). We calculated the corrections using an additional EC system in the study site that had been installed over a plane surface [58]. Using measurements of Swin radiation at the reference site, the incoming solar radiation for an inclined plane (SW $_{\psi}$) can be calculated by applying the following equation, as described by [57]:

$$SW_{\psi} = SWexp \left[-kt(\psi^2 - \theta_z^2) \right] \left[1 + Asin^2 \left(\frac{\psi}{2} \right) \right] \tag{1}$$

Here, kt values were calculated using the ratio of SW and estimates of the extra-terrestrial radiation and A values were calculated using Swin and Swout measurements from the net radiometers, the solar zenith angle (θz), and the angle between the horizontal and the inclined surfaces, and the direction of the sun using NOAA's Solar Calculator based on astronomical algorithms [59]. Similarly, Lwin, Lwout, and Swout were also corrected for calculation of Net Radiation, which was as follows:

$$Rn = Swin + Swout + Lwin + Lwout$$
 (2)

2.6. Heat and Moisture Changes in Canopy Air

At 4 different height levels above ground, i.e., level 1 = 1 m, level 2 = 7 m, level 3 = 12.5 m, and level 4 = 19 m, we installed low-budget temperature/relative humidity sensors to estimate the vertical heat and moisture development in the diurnal cycle. The changes along the profile in the understory air were made to test the storage effect of the forest ecosystem, which contributed to the overall estimation of the quality of the fluxes. The data were normalized based on the air temperature (Ta) and relative humidity (RH) measurements

Forests **2024**, 15, 1828 7 of 22

above canopy obtained from the EC system. This ensured a consistent comparison of heat and moisture variations within the canopy air. The normalized values were defined thus:

$$Ta_{i,norm} = \frac{Ta_i}{Ta} \tag{3}$$

$$RH_{i, norm} = \frac{RH_i}{RH} \tag{4}$$

 Ta_i and RH_i were the temperature and relative humidity obtained by the low-budget sensors, i was the value at the respective height level (1, 6, 12.5, 19 m), and Ta and RH were the above-canopy temperature and relative humidity obtained by the EC system. The resulting normalized values provided an overview of above/below values compared to the reference, i.e., EC level conditions.

To quantify the heat and moisture storage integrated between 0 m agl. and canopy height ($z_c = 25$ m), we used the theoretical definition also described in [35]. It is defined thus:

$$S_H = \rho_a \cdot c_p \int_0^{z_c} \frac{\partial T}{\partial t} dz \tag{5}$$

$$S_{LE} = \rho_v \cdot L \int_0^{z_c} \frac{\partial RH}{\partial t} dz \tag{6}$$

 S_H and S_{LE} represent storage (S) of sensible heat (H) and latent heat (LE), ρ_a and ρ_v represent air density for dry and wet air, c_p represents the specific heat capacity, L is the latent heat of vaporization, and z_c is the canopy height (25 m). Written as finite differences and summarized over the time increment $\Delta t = 30$ min, we derived the following:

$$S_H(t) = \sum_{i=1}^n \rho_a \cdot c_p \cdot \frac{Ta(z_i, t) + \Delta t) - Ta(z_i, t)}{\Delta t} \cdot \Delta z_i$$
 (7)

$$S_{LE}(t) = \sum_{i=1}^{n} \rho_v \cdot L \cdot \frac{RH(z_i, t) + \Delta t) - RH(z_i, t)}{\Delta t} \cdot \Delta z_i$$
 (8)

Here, t is time, Δt is time increment, and z_i represents the respective height levels (1, 6, 12.5, 19 and 25 m).

3. Results

3.1. Wind Field

Mountainous regions are highly dominated by slope winds developed in the diurnal cycle and affecting the planetary boundary layer (PBL). Because of the location of the EC system, we start our analysis by looking particularly at this mechanism and its impact on the turbulent fluxes. Figure 2 shows the wind field (speed and direction), u^* , and the Monin–Obukhov stability parameter ((z - d)/L).

Generally, a clear diurnal cycle could be observed for each variable illustrated, which pointed to the occurrence of changing wind fields in the diel. The wind direction was rapidly changing, especially in the transition between daytime and nighttime hours. While, from 9:00 to 17:00, the north-eastern direction (35–65 degree) dominated, representing upvalley flows, the dominant direction changed to a south-eastern direction (155–175 degree) from 18:00 to 7:00, indicating down-valley flows. The slope valley winds tended to be stronger during the late morning and afternoon hours as the irradiance created the stronger gradients. This was reflected in the wind speed and u* as well. They featured the highest (lowest) values from 9:00 to 17:00 (7:00–8:00), being associated with the strongest (weakest) variability. During the daytime, the wind speed ranged from 4 to 6 m/s while, during the nighttime, it declined down to 2.5 m/s. The maximum wind speed of 9 m/s was observed at 12:00 with a corresponding strong u* of 2.10 m/s, creating strong turbulent mixing. The situation changed during the nighttime, when calm conditions predominated and mixing

Forests **2024**, 15, 1828 8 of 22

was weakened, as indicated by u* varying between 0.1–0.75 m/s. Further, the variability of both wind speed and u* was distinctly reduced during nighttime hours.

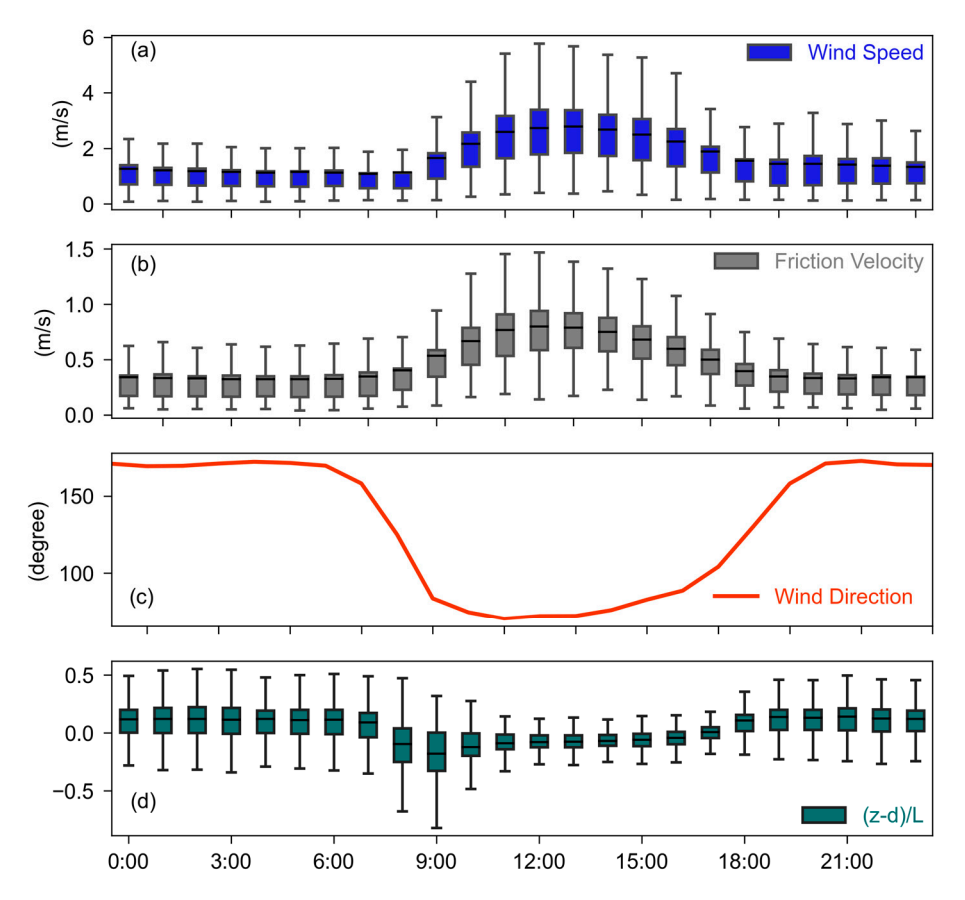


Figure 2. Mean diurnal course of meteorological variables from January 2020 to December 2022: (a) wind speed (m/s, boxplot, blue), (b) friction velocity (u* m/s, orange), (c) wind direction (degree, blue), and (d) Monin–Obukhov stability parameter ((z - d)/L), blue).

The Monin–Obukhov stability parameter ((z-d)/L) confirmed the variations in the turbulence activities from the surface to the canopy in the diurnal cycle. The lower atmosphere was mostly turbulent during the late morning period (08:00–09:00), as indicated by the strongest negative values ranging from -0.2 to 0.2. This was the hour of the day when the wind direction was changing and the speed was increasing, resulting in the development of neutral and unstable PBL conditions (values ≤ 0) during the daytime. The atmospheric stratification was modified to stable conditions (values > 0) during the nighttime with mostly positive values. Fluctuations towards negative values could also be observed due to down-valley winds, which induced turbulent kinetic energy (TKE) within the NBL [20,21].

3.2. Vertical Heat and Moisture Effects

As it is well known, forest ecosystems evolve a storage effect due to differences in the vertical energy transportation within the understory and at the canopy [60,61]. Storage effects within the canopy related to air temperature and relative humidity involve the retention and exchange of heat and moisture within the canopy and surface layers, which feed back to the ecosystem's energy balance. In terms of the rate of CO_2 flux, it was determined by the difference between the instantaneous profiles of concentrations at the beginning and end of the 30 min EC averaging period, which was divided by the averaging period itself [60,62]. During nighttime, when the atmosphere was stable stratified and turbulence was weak, the storage effect became important as it may have exceeded the CO_2 fluxes. For this, as mentioned above, we installed four low-budget sensors at different

Forests **2024**, 15, 1828 9 of 22

height levels within the canopy to estimate a storage capacity concerning air temperature and relative humidity profiles.

Figure 3 illustrates the storage capacity for heat and moisture calculated based on Equations (3) and (4) normalized values > 1 (<1) indicate higher (lower) values than those above the canopy at the EC measurement level (z_c) while 1 represents equal values. This means that unstable, stable, and neutral stratifications could be derived. Generally, the strongest temperature deviations were developed during daytime while the nighttime hours oscillated around 1 (Figure 3a). With the exception of level 1, warmer Ta occurred during the daytime, particularly for level 3 and 4. Here, higher values than those above the canopy between 15% (1.15) and 25% (1.25) rapidly developed in the morning hours and remained over the day. The lowest level (1 m agl), in contrast, showed below-reference values down to 10% (0.9), which indicated cooling effects near the ground. Height level 2 fluctuated around 1 throughout the day, with the highest values being from the afternoon (13:00-16:00) and lowest values being from around the early evening (17:00-18:00). RH illustrated the opposite behavior, with the highest deviations being from reference in 1 m (>60%) around noon (Figure 3b), which represented an accumulation of moisture near the ground. Level 3 and 4, on the other hand, were close to 1 and below the reference, which pointed to drier conditions than those above the canopy.

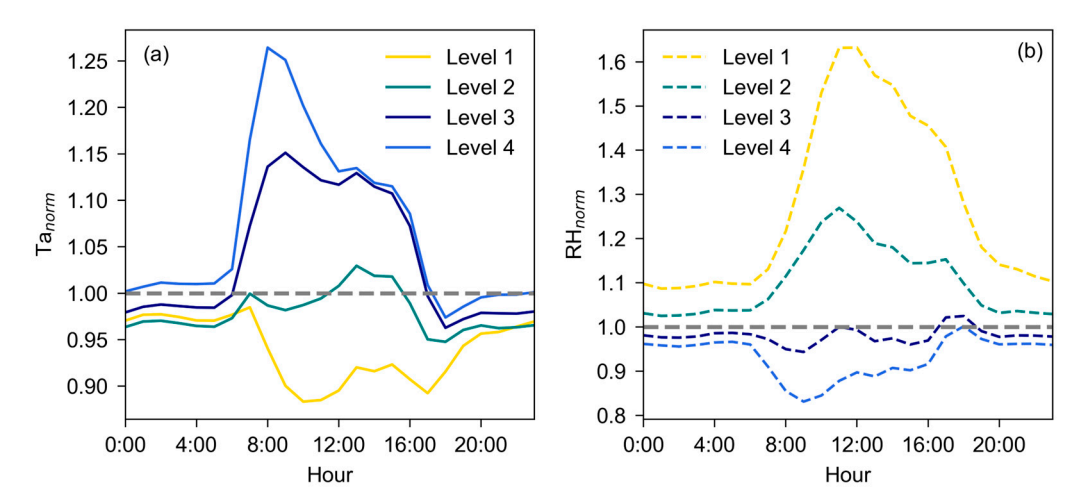


Figure 3. Diurnal course of storage capacity indicated by (a) normalized air temperature (Ta_{norm}) and (b) normalized relative humidity (RH_{norm}) at height levels 1 = 1 m, 2 = 6 m, 3 = 12.5 m, and 4 = 19 m.

3.3. Energy Balance Closure

One of the greatest challenges involved in EC measurements, particularly in sloped and heterogeneous terrain, is finding the EBC, as described by various authors [27,33,63]. However, it offers a possibility to validate EC measurements by the sum of LE and H against the difference between the net radiation (Rn) and ground heat flux (G) through linear regression analysis [17,64]. It is defined thus:

$$Rn = LE + H + G + \varepsilon \tag{9}$$

 ε is the residual flux, representing the imbalance.

Figure 4a shows the EBC with an explained variance of R^2 = 0.795, which characterizes a good closure and is in the range of uncertainty in complex terrain [31]. In order to explore the behavior of the energy fluxes, Figure 4b shows the mean diurnal cycle of H and LE, in which Rn and the corrected net radiation (Rn*) are also examined. As expected, the energy fluxes resembled a strong diurnal cycle with a peak around noon and a decline at night. LE was the strongest contributor to the energy exchange at our site, with a mean maximum of 400 W/m^2 , while H reached 200 W/m^2 . Interestingly, G revealed a lag in its peak phase for both daytime and nighttime hours.

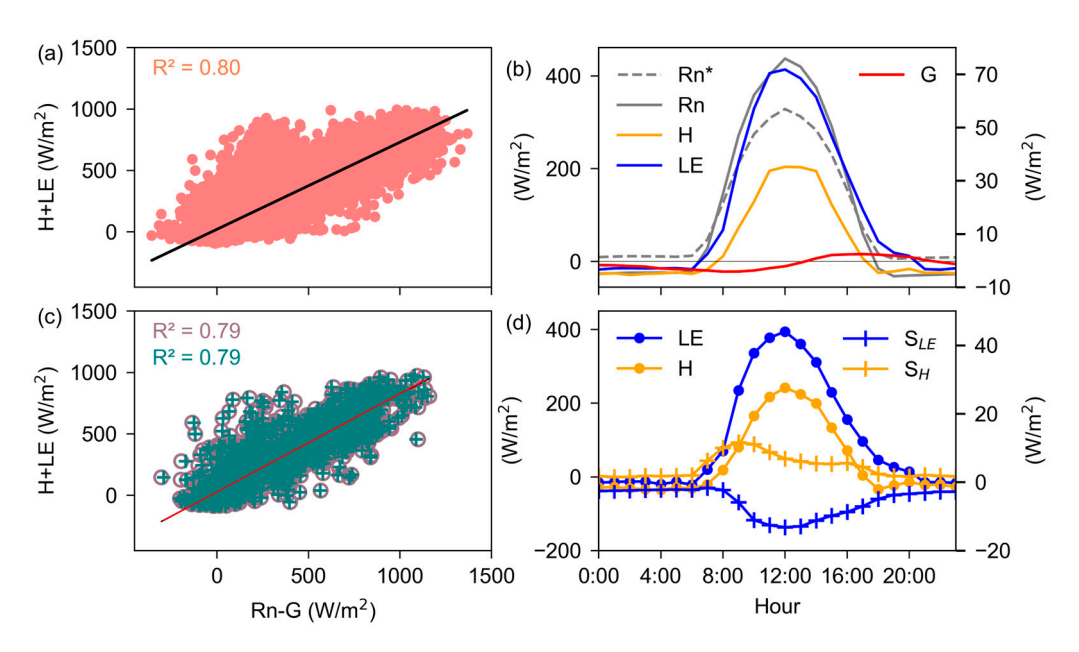


Figure 4. (a) Linear fit of the sum of sensible heat $(H, W/m^2)$ and latent heat $(E, W/m^2)$ against net radiation $(Rn, W/m^2)$ minus ground heat flux $(G, W/m^2)$; (b) diurnal cycle of LE (dark blue, W/m^2), H (orange, W/m^2), G (red, W/m^2), corrected net radiation $(Rn^*$, solid blue line, W/m^2), and uncorrected net radiation $(Rn, dashed blue line, W/m^2)$ for the time period January 2020–December 2022; (c) same as (a), without the addition of the storage effect and with storage effect; (d) diurnal cycle of turbulent energy fluxes without storage (LE and H, W/m^2) and with addition of storage $(S_{LE} \text{ and } S_H, W/m^2)$ for the time period October–December 2022.

To reduce uncertainties in the EBC, we corrected Rn as described by [32,39,40]. Comparisons between Rn and Rn* illustrated that the corrections applied clearly affected the magnitude of the radiation budget (Figure 4b). While Rn reached a maximum of 450 W/m^2 during the daytime, Rn* exhibited a reduced magnitude (320 W/m^2). For the nighttime, this behavior was changed and Rn featured a stronger radiation loss than Rn*. The most significant modifications occurred in the morning hours as well as during the daytime. Although both Rn and Rn* peaked at noon, the latter resembled a more smoothed pattern. Despite these adjustments, the overall improvement in the EBC was only marginal as indicated by $R^2 = 0.795$ (Rn) in comparison to $R^2 = 0.794$ (Rn*). Since the magnitude of Rn* was consistently lower than the LE, and since the accuracy of the EBC has not been improved significantly, the uncorrected values are used in the ongoing analyses.

Considering the effect of storage on heat (S_H) and moisture (S_{LE}) exchange, the EBC and diurnal cycle of LE and H have additionally been included for the time period October 2022–December 2022 (Figure 4c,d). When storage is added, improvements in the EBC from $R^2 = 0.786$ to 0.789 and in the root mean square error (RMSE) from 121.37 to 120.37 are achieved (Table 2). Although the effect is only marginal, the diurnal cycle, in particular, reveals an important insight into systematic patterns.

Table 2. Linear fits, explained variance (R^2), and root mean square error (RMSE) of the sum of sensible heat (H, W/m²) and latent heat (LE, W/m²) as functions of available energy (Rn -G, W/m²) for H and LE without storage and with the addition of storage for the time period October 2022–December 2022.

| | Intercept | Slope | R ² | RMSE |
|--------------------------|-----------|-------|----------------|--------|
| Without storage | 27.71 | 0.79 | 0.786 | 121.37 |
| With addition of storage | 27.20 | 0.80 | 0.789 | 120.37 |

Table 3 summarizes the mean and integrated storage effects related to the mean diurnal cycle, as well as to the daytime, nighttime, and transition hours as defined in Table 1. In

Forests 2024, 15, 1828 11 of 22

total, on a daily basis, S_H and S_{LE} accounted for 4.4 and $-5.6 \,\mathrm{W/m^2}$, respectively. When we take a look at the hours of day, it can be observed that H generated an overestimation of heat (S_H) of more than 10 W/m², especially from 8:00 to 10:00, with a subsequent decline from noon down to 5.5 W/m², when mixing was strongest. For LE, an underestimation occurred, as indicated by the negative values of S_{LE} . It reached its lowest values from 10:00 to 14:00 with around $-12 \,\mathrm{W/m^2}$. As integral values, S_H and S_{LE} accounted for 105.2 and $-133.7 \,\mathrm{W/m^2}$, respectively, 55% and 40% of which were generated in the transition hours.

Table 3. Mean and sum of the storage effect generated by the sensible heat flux (S_H , W/m²), latent heat flux (S_{LE} , W/m²), and EBC residual (ε , W/m²), calculated over the diel (all), daytime, nighttime, and transition hours as defined in Table 1 for the time period October 2022–December 2022.

| | S_H (W/m ²) | | S_{LE} (W/m ²) | | ε (W/m ²) | |
|------------|---------------------------|-------|------------------------------|--------|-----------------------|-------|
| | Mean | Sum | Mean | Sum | Mean | Sum |
| All | 4.4 | 105.2 | -5.6 | -133.7 | 14.8 | 356.2 |
| Day | 6.8 | 27.1 | -12.5 | -49.9 | 56.9 | 227.8 |
| Night | 1.8 | 19.5 | -2.6 | -28.5 | 6.5 | 71.9 |
| Transition | 6.5 | 58.5 | -6.1 | -55.1 | 6.3 | 56.5 |

3.4. Energy Balance Closure as a Function of Time

As the diurnal cycle of the storage capacity (Figures 3 and 4) revealed variations in heat and moisture during daytime (11:00–14:00), nighttime (20:00–6:00), and transition (7:00–10:00, 15:00–19:00) hours, we additionally established the EBC for these time periods. Table 4 summarizes both the linear regression coefficients as well as the $\rm R^2$ and RMSE values.

Table 4. Linear fits, explained variance (R^2), and root mean square error (RMSE) values of the sum of sensible heat (H, W/m²) and latent heat (LE, W/m²) as a function of available energy (Rn -G, W/m²) for day (11:00–14:00), night (20:00–6:00), and transition (07:00–10:00 and 15:00–19:00).

| Time Period | Intercept | Slope | R ² | RMSE |
|-------------|-----------|--------|----------------|--------|
| All data | 20.59 | 0.79 | 0.795 | 107.29 |
| Day | 135.8 | 0.56 | 0.545 | 133.32 |
| Night | -31.19 | -0.005 | | 22.17 |
| Transition | 33.39 | 0.67 | 0.666 | 108.36 |

The results confirm a clear decrease in EBC during the day ($R^2 = 0.545$) while, in the transition, the explained variance increased to $R^2 = 0.666$. This was also reflected in the RMSE with 107.29 against 133.32 for daytime and 108.36 for the transition hours.

With respect to the ε of the EBC, differences between daytime and nighttime imbalances could be observed for both the entire time period and the sub-period related to the storage effect (Figure 5, Table 3). Basically, during nighttime, on average, imbalances were close to zero. As the morning hours, associated with global radiation (Rg), approached, an underestimation of approximately $50~\text{W/m}^2$ on average occurred. This was rapidly modified to an overestimation in the late morning hours of around $140~\text{W/m}^2$ and peaked prior to the energy flux maxima before declining in the afternoon. Thus, variations in the EBC developed in the diurnal cycle. This was also true for the shorter time period. Comparing ε and ε' , it can be observed that the addition of the storage effect in H and LE (S_H and S_{LE}) reduced the imbalances. However, when the data are divided into the three time periods, it can be noted that daytime hours contributed the most to the imbalances, accounting for 64% of the total amount ($356.2~\text{W/m}^2$).

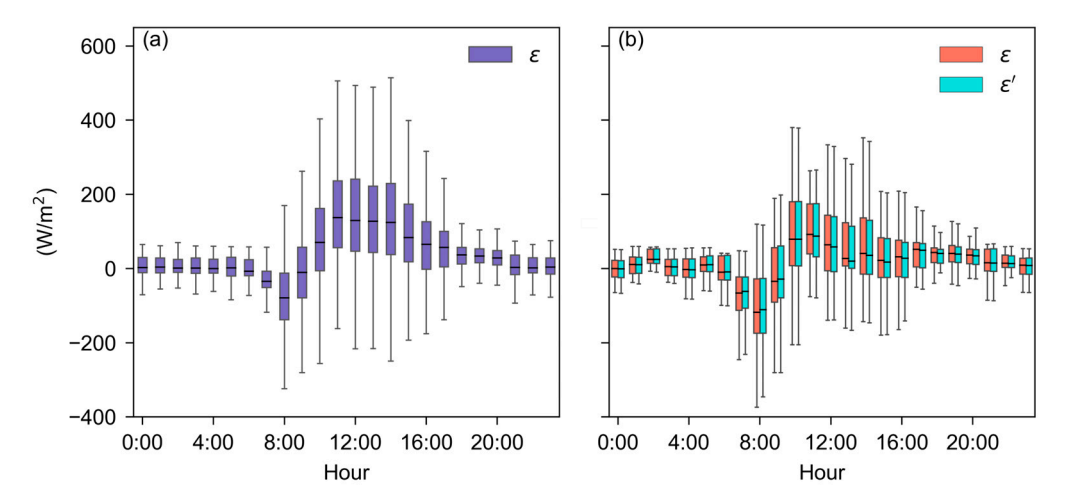


Figure 5. Boxplots representing the diurnal course of (**a**) the residuals (ε , W/m², purple) for the time period January 2020–December 2022 and (**b**) the residuals without storage values (ε , W/m², red) and with addition of storage (ε' , W/m², cyan) for the time period October–December 2022.

As observed in Figures 1 and 2, the wind direction changed significantly in the diurnal cycle. When we take a look at the impact of the wind direction on the EBC (Figure 6), it is obvious that ε tended to increase with wind directions between 0–100° and 200–250°. While, in the north-eastern direction, the under-/overestimation ranged between –400 to 700 W/m², the south-western direction mostly contributed to an underestimation down to –600 W/m². In both cases, this was particularly true during the transition from daytime to nighttime. The morning hours and transition between nighttime and daytime, in contrast, contributed, rather, to an underestimation of the residuals. During the nighttime, ε values ranging between –200 and –400 W/m² were associated with directional changes in the wind field between 100° – 200° and 250° – 330° .

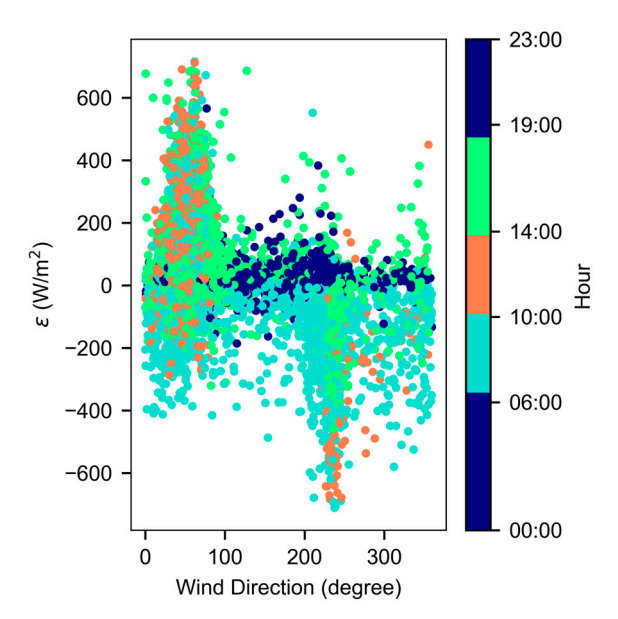


Figure 6. Scatter plot showing residuals $(\varepsilon, W/m^2)$ and wind directions (degrees), with the markers representing different time periods of day at daytime (orange), transition (green), and nighttime (blue) as defined in Table 1.

We also examined the relationship between the wind direction and S_H and S_{LE} for the period from October 2022 to December 2022 (Figure 7). Again, wind directions approximately in the ranges of 0–100° and 200–250° caused the largest storage effects in H and LE. In particular, the north-eastern direction leads to the strongest over-/underestimations,

ranging between -25 to 5 W/m^2 for S_{LE} and up to 25 W/m^2 for S_H . During nighttime hours, the storage effects were rather low and oscillated between -6 to -0.4 W/m^2 and -3 to 10 W/m^2 for S_{LE} and S_H , respectively. Similar to what can be observed in Figure 6, LE was overestimated, ranging from 8 to -26 W/m^2 , when the wind direction had a north-eastern component, particularly during the peak of the day and transition periods. In contrast, H was underestimated during these periods, with values ranging from -3 to 26 W/m^2 . Wind directions between $210 \text{ and } 250^\circ$ also showed an overestimation of H, but with a lower magnitude compared to $30\text{--}100^\circ$. In this case, S_{LE} ranged from -20 to 6 W/m^2 while S_H ranged from -4 to 20 W/m^2 .

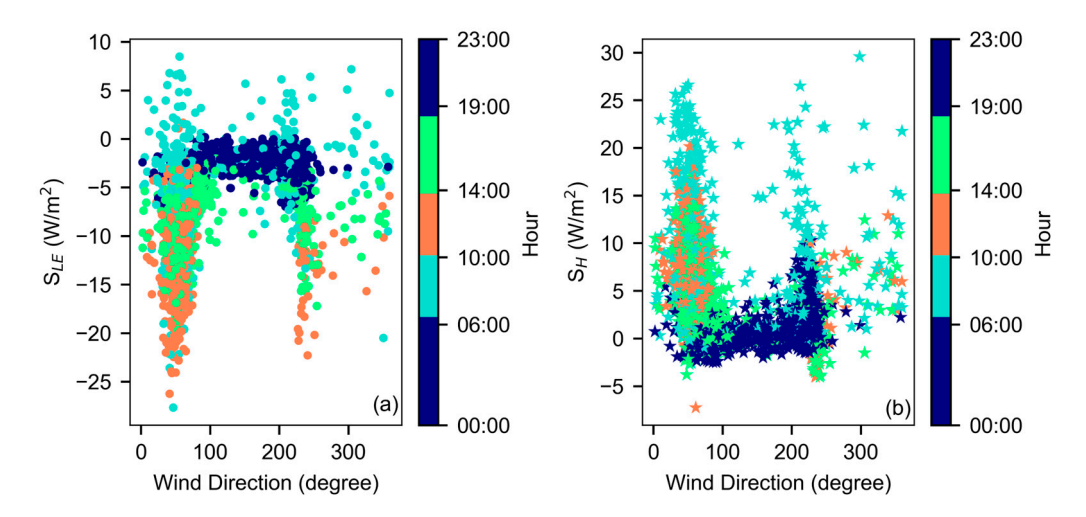


Figure 7. Scatter plots between of (a) S_{LE} (o, W/m^2) and (b) S_H (*, W/m^2), with wind direction (degree) values shown. The markers represent different time periods of day at daytime (orange), transition (green), and nighttime (blue) as defined in Table 1 for the time period October–December 2022.

3.5. Energy Balance Closure and Its Relation to Thermodynamic Conditions

In order to shed light on the relation between imbalances and thermodynamic conditions and turbulence activities, Figure 8 displays (z-d)/L and u^* against ϵ . Since both the residuals without and with the addition of the storage effect were comparable, the former ϵ is used in the ongoing analyses. The data were binned into 20 classes. As a result of averaging over each bin, but to highlight the varying signals, the y axis differed between u^* and (z-d)/L.

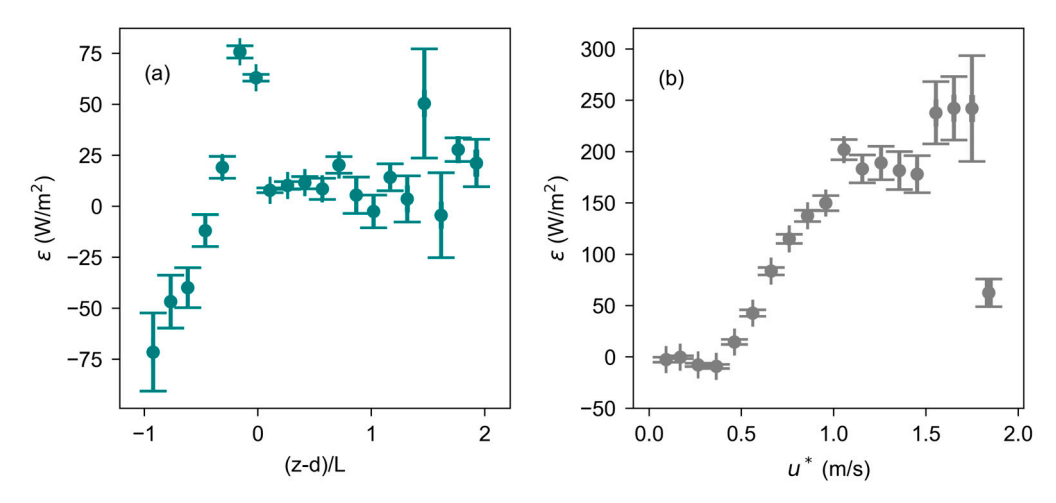


Figure 8. Binned means of residuals $(\varepsilon, W/m^2)$ as functions of **(a)** Monin–Obukhov stability parameter (z - d)/L and **(b)** friction velocity $(u^*, m/s)$. Axis has been subjected to differ for subplots.

Based on the stability parameter, a clear relationship between an underestimation of the energy balance and unstable conditions could be observed as ε reached values down to $-75~\rm W/m^2$. In contrast, weak-unstable to neutral conditions were associated with the strongest overestimation up to $75~\rm W/m^2$. During stable stratifications, ε was close to zero but increased towards a strong stable stratified PBL with an additional higher variability. With respect to u*, weak values between 0.1 and 0.5 m/s featured small imbalances while they increased with stronger u* values, resulting in large overestimations. Reaching a u* value of more than 1.8 m/s, ε decreased sharply down to $50~\rm W/m^2$.

Separated into the three time periods of the day (Table 1), and also visible in Figure 5, variations in the amount of imbalances could be recognized. Figure 9 illustrates that daytime imbalances varied between the strongest overestimations (100 W/m²) during weak-unstable to neutral conditions (-1 < (z-d)/L < 0.5) and strongest underestimations (-100 W/m²) during weak stable conditions ((z-d)/L > 1). Nighttime, in contrast, generated a rather small overestimation (5-50 W/m²) of the EBC independent of the stability while the transition time revealed a clear relationship between the thermodynamic stability and ε . Imbalances as a function of u* reflected a similar behavior, pointing to the turbulence activity. During the daytime, when the strongest mixing occurred (u* > 0.5 m/s), overestimations were largest (up to 250 W/m²) while nighttime hours represented calm conditions with the smallest ε values varying slightly between positive and negative imbalances (-30-20 W/m²). In the transition time, when mixing was modified, imbalances changed from under- to overestimation at around -50-50 W/m².

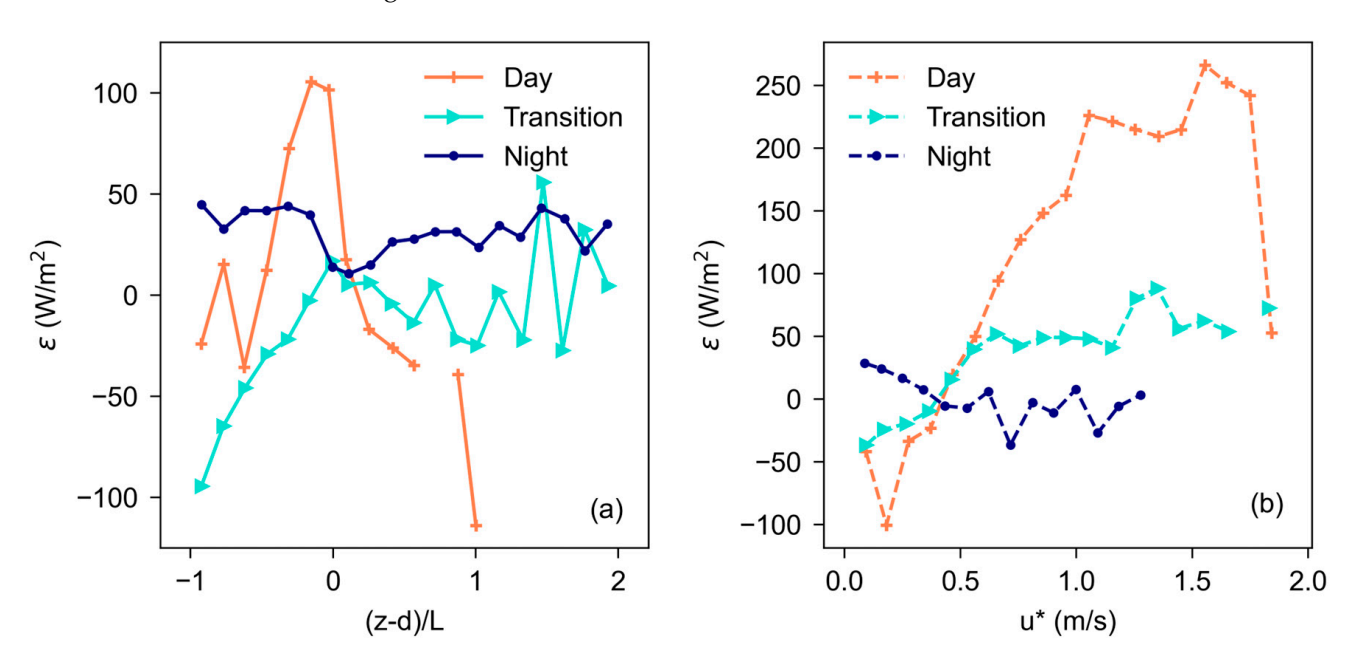


Figure 9. Relationships of residuals (ε , W/m^2) with (a) stability parameter ((z - d)/L, solid) and (b) friction velocity (u^* , dashed) during daytime (orange line), transition (green line), and nighttime (blue line) as defined in Table 1.

Considering the relationship between ϵ and Rn as a function of (z-d)/L and u^* , it can be observed that the strongest overestimations of the energy balance were associated with higher irradiance. This was particularly true for the stability parameter, which revealed the peak phases for weak-unstable to neutral conditions. According to u^* , Rn peaked with $350~W/m^2$ between 0.5 and 1.0~m/s in Figure 10. Interestingly, the strongest imbalances $(250~W/m^2)$ occurred during lower irradiance levels of around $100~W/m^2$, representing, again, the transition hours of the day.

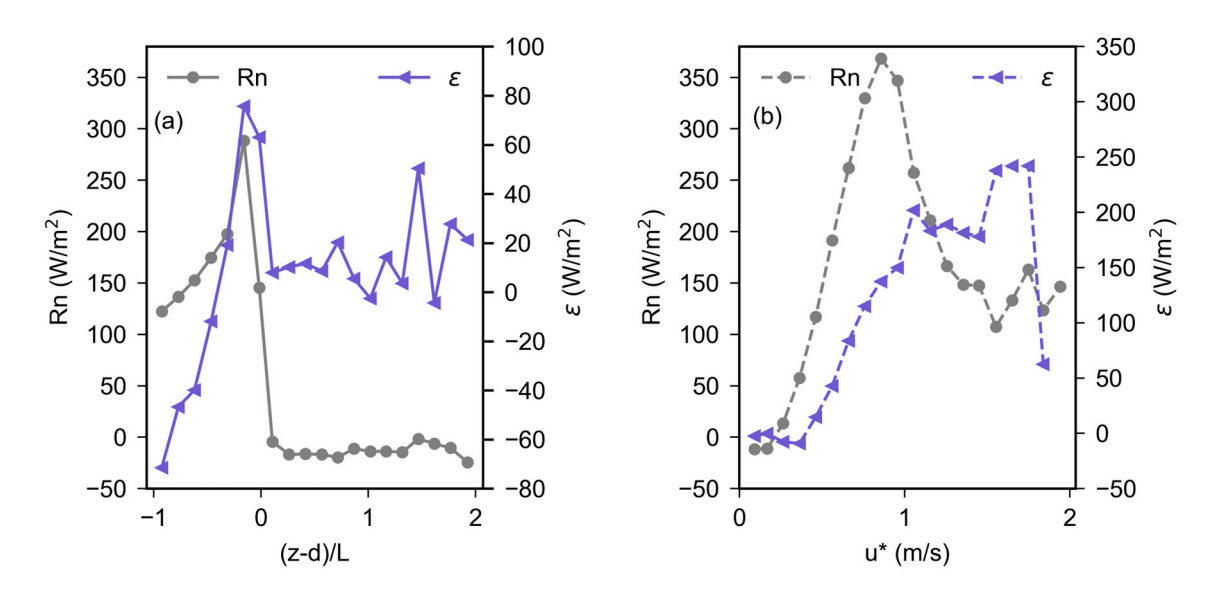


Figure 10. Binned means of residuals $(\varepsilon, W/m^2)$ and net radiation (Rn, W/m^2) as functions of (a) Monin–Obukhov stability parameter (z - d)/L and (b) friction velocity $(u^*, m/s)$.

3.6. Diurnal Cycles of CO₂ Fluxes

Our next step is to examine the NEE estimated based on the CO_2 flux measurements by the EC system. Because the data encountered similar challenges regarding the data quality as the energy fluxes, careful inspection is required as well. Thus, we explicitly analyze the unfiltered NEE and filtered NEE (NEE*) to identify the impact of local wind systems and precipitation events on the carbon fluxes. The diurnal patterns of the NEE and NEE* highlight the dynamic nature of CO_2 exchange within the ecosystem. Understanding these patterns is crucial for assessing the carbon balance and the role of the ecosystem.

Figure 11 shows the typical diurnal cycle of the NEE and NEE*, with positive values during the morning period indicating CO_2 respiration and negative values during daytime indicating the absorption of CO_2 by the canopy. The maximum absorption of CO_2 was observed between 11:00 and 12:00, with values ranging from NEE = -40 to $-49~\mu mol/m^2/hour$. This peak indicated the highest photosynthetic activity within the canopy during this period. A noticeable shift in the NEE during the upwind period was observed between 7:00 and 8:00. During this period, maximum turbulence was seen as indicated in Figure 2d, with the NEE shifting from 0.4 to $-5~\mu mol/m^2/hour$. This turbulence likely enhanced the mixing and, thus, the transport of CO_2 within the canopy. A change in the NEE from negative ($-3.21~\mu mol/m^2/hour$) to positive ($5~\mu mol/m^2/hour$) was observed during the downwind period between 17:00 and 18:00 and represented a transition from CO_2 uptake to release as the photosynthetic activity decreased and respiration became dominant.

With respect to the correction, a difference could be detected in the magnitude of the NEE. The magnitude changed from NEE = $-1.4~\mu mol/m^2/day$ to NEE* = $-5.90~\mu mol/m^2/day$, which was also reported by [2]. During the stable conditions, the underestimation of the NEE occurred. Discarding such data necessarily minimizes the impact on the NEE due to stable conditions [38]. Implementing u* filtering helps remove periods of insufficient turbulence, thereby reducing the potential bias in nocturnal flux measurements. This leads to a more accurate assessment of ecosystem respiration during nighttime. This filtering is particularly important for avoiding biases in nocturnal flux measurements and improving the overall quality and reliability of the data used in carbon budget analyses [18,55]. The primary goal of these corrections in this study was to prepare the data for subsequent processes such as gap filling and partitioning, which are crucial steps for ensuring a dataset's usability.

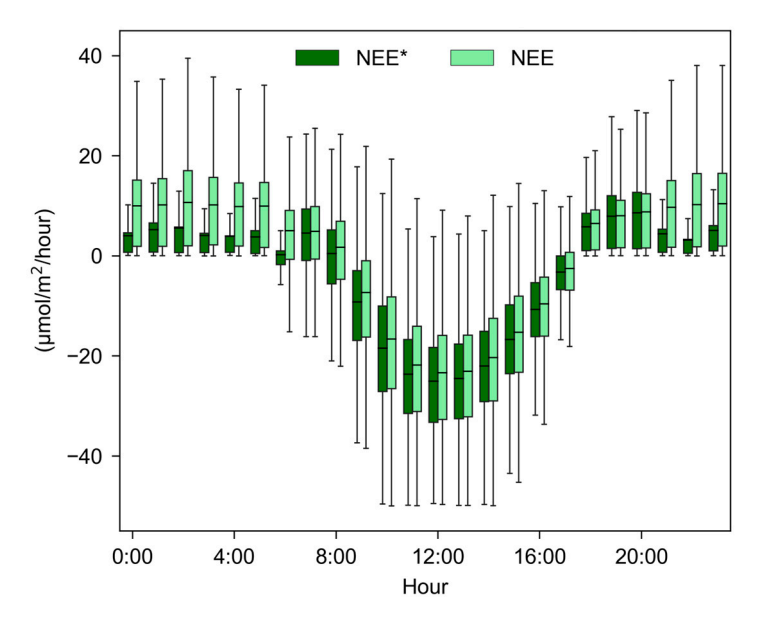


Figure 11. Boxplot representing diurnal course of unfiltered net ecosystem exchange (NEE, solid line, μ mol/m²/hour) and filtered NEE* (dashed line, μ mol/m²/hour) for the entire time period.

3.7. Light-Response and Carbon Exchange Model

To independently model the NEE and explore the ability to estimate carbon fluxes in such a challenging environment, Figure 12 illustrates the non-linear fit of the daily NEE* as a function of Rg and PPFD from 8:00 to 16:00 to ensure full irradiance. The latter was only available for the time period March–December 2022. The non-linear fits for both Rg and PPFD resembled typical saturation curves with the strongest CO_2 uptake (NEE* = $-18~\mu mol/m^2/day$) being around 400 W/m² and 80 mol/m²/day, which represented the maximum uptake by the ecosystem under optimal light conditions. Since both models showed R^2 values of 0.51 and 0.49 with Rg and PPFD, respectively, a good performance of the carbon exchange model existed. Thus, the variance of the NEE can be estimated with independent meteorological quantities, which points to a sufficient quality of CO_2 fluxes. We also tested the correlation of the uncorrected NEE, which resulted in a weaker relationship, especially with PPFD (0.48), while Rg showed 0.49.

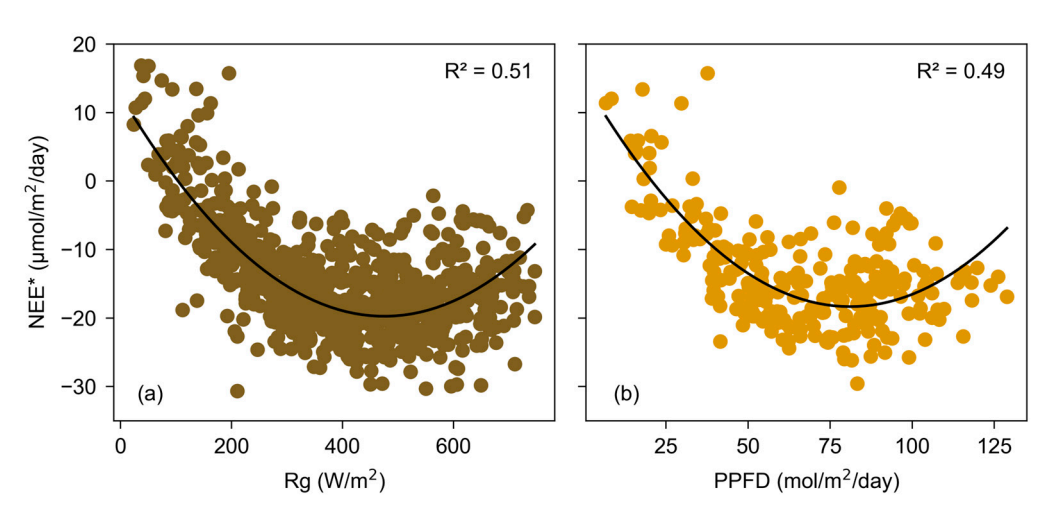


Figure 12. Relationship between net ecosystem exchange (NEE*, μ mol/m²/day) and (a) global radiation (Rg, W/m²) and (b) photosynthetic photon flux density (PPFD, mol/m²/day). Daily means are used for analysis for specific time period between 8:00–16:00. Rg data span the entire period (January 2020–December 2022) while PPFD data are limited to the period March 2022–December 2022.

Forests **2024**, 15, 1828 17 of 22

4. Discussion

In this study, we used energy and carbon fluxes obtained by an EC measurement system above a forest canopy in complex terrain of the tropical Andes Mountains in southern Ecuador. The main aim was to investigate the impact of both the terrain as well as the vegetation height on the turbulent exchange of momentum, energy, and carbon fluxes essential to quantify uncertainties in the energy balance and the heat storage effect. In such complex areas, flux measurements are affected by thermally driven wind fields in the diurnal cycle. Additionally, the EBC and its residuals were analyzed and reflected in the diurnal cycle with respect to the heat storage generated by the forest ecosystem to quantify the quality of the measurements in this challenging environment.

As expected, the study site was influenced by the local wind systems that had developed in the diurnal cycle (Figure 2). This means, that during daytime hours, an upslope flow could be observed while in the nighttime hours, it was reversed to a downslope flow due to net radiation loss. The consequences were varying wind speeds and turbulence activities. The latter were confirmed by the Monin–Obukhov stability parameter ((z - d)/L). Here, it was revealed that during the nighttime, stable stratified atmospheric conditions dominated (values > 0) while during the daytime, the dominant condition alternated between neutral (values = 0) and unstable stratified conditions (values < 0). However, in particular, the transition from nighttime to daytime showed the strongest variability with values down to -0.7. During that time of the day, air masses in the downslope flow changed their direction to upslope, which created turbulent activities and a destabilization of the PBL. Advection occurred in the nighttime hours, where downslope flows led to alterations between stable and neutral conditions as indicated by u* reaching up to 1.5 m/s and (z - d)/L fluctuating from 0 to >0.5, which had also been mentioned by [25,28,30,65].

The storage effect was estimated on the basis of both heat and moisture profiles within the canopy as well as S_H and S_{LE} (Figures 3 and 4). The normalized Ta/RH values in the diurnal cycle revealed the strongest deviations from the reference level (z_c) at the highest levels in the understory (level 3 and 4) during morning hours (7:00–10:00). That means that during the transition to daytime and incoming radiation, an accumulation of heat and moisture, which is and was not mixed downward. At the same time, the strongest turbulence activities above the canopy were revealed, and these evolved into an upward mixing into the atmosphere. The lowest level, on the other hand, was below z_c , pointing to an exchange with the soil and stable stratified conditions. From 11:00, when mixing was fully developed as indicated by the maximum of u^* , the wind speed and (z-d)/L differences between Ta_{norm} and RH_{norm} were reduced for levels 3 and 4, but level 1 showed only weak changes. However, differences between the lower and upper levels highlighted the influence of the sloped terrain and the vegetation height on the stratification of the air mass column and the storage capacity.

The unstable stratification and energy storage generated high EBC residuals as illustrated in Figures 4 and 5. The EBC, in total, showed a good performance at the study site ($R^2 = 0.795$) as also described by [23] for tropical rainforest ecosystems in complex terrain. For instance, [40] studied a dry forest ecosystem with complex terrain and found EBC values that varied with seasonality, showing an R^2 ranging between 0.77 and 0.9. The authors of [66] reported an EBC of 87% at a site with less complex terrain but an evergreen forest, which was higher than the average for those sites. Similarly, for a tropical evergreen forest in China, [67] reached an EBC of 75%. These comparisons suggest that our site's EBC was within the expected range for ecosystems with similar characteristics.

Moreover, our EBC could marginally be improved for a shorter time period considering the heat storage effect of the forest, which is in agreement with [68]. The authors additionally calculated the storage effect of the biomass for individual sites, which improved the EBC more significantly. In our case, we only could consider the storage effect related to H and LE. In the diurnal cycle, it could be demonstrated that S_H imposed a positive effect, i.e., the accumulation of heat, especially in the morning transition period, while S_{LE} featured an opposite pattern with a time lag towards late morning hours. Again,

the storage effect predominately evolved during the transition time (40%–55%) as already observed using the normalized Ta/RH values.

The performance of the EBC also followed the diurnal cycle. While ϵ was largest during the daytime hours (overestimation) when strong unstable conditions lead to strong mixing, the nighttime hours were associated with stable conditions and weak turbulence, generating fewer imbalances (Figure 5). Most likely, the increase in ϵ during daytime was induced by vertical flux divergence as a result of strong upslope flows as described by [28]. Due to the heterogeneity of the topography that those mountain breezes frequently develop, [30] demonstrated that these topographical characteristics cause large eddies that enhance LE as a result of the non-local transport of heat and moisture.

The wind shifted during the transition period, driven by upslope and downslope flows, resulting in higher residuals. However, the complex terrain also contributed to advection during this period, leading to a phase difference in wind direction signals, as shown in Figure 1. Additionally, while the residuals (ε) were highest during these periods, they were not limited to phase shifts. Elevated residuals were also observed from other wind fetch directions and during different time periods, as seen in Figure 6. Furthermore, other factors that contributed to the general lack of energy balance closure in flux studies, unrelated to advection, were not addressed in this investigation but likely still played a role. We used the EB closure (EBC) as an indicator of flux quality, but it is important to consider these other factors when interpreting the results of any filtering or correction scheme applied to the flux data, as discussed by [40].

The transition in the morning hours was characterized by an underestimation down to -80 W/m^2 on average, when weak unstable conditions evolved. This was also shown by [35], who pointed to stronger imbalances especially during the daytime and transition rather than during nighttime hours [27].

Reasons for the varying imbalances were demonstrated using (z - d)/L and u^* (Figures 7 and 8). Generally, a shift from underestimation to overestimation was observed in association with atmospheric stratification. Very unstable conditions ((z - d)/L < -1.0) were related to an energy deficit while weak unstable and very stable conditions ((z-d)/L > 1.5) led to overestimations. The relationship between ε and u^* highlighted that imbalances increased with turbulence activities. With the data divided into the three time periods, it can be noted that the largest imbalances (under- and overestimation) evolved during the day. With the fully developed PBL during the daytime, an overestimation of up to 100 W/m² on average occurred as the conditions were unstable and turbulence activities were strongest (u* > 0.5 m/s). This is explained by more low-frequency turbulences (i.e., larger eddies) occurring due to the occurrence of organized convection and the development of a deeper PBL [63]. Nighttime hours showed a weak overestimation across the stratifications. Typically, underestimations occur due to the development of the NBL and stable conditions. At our site, we could observe that fluctuations in u* values and (z - d)/L appeared, which induced mixing contrary to the expected calm conditions [69]. Further, the micrometeorological conditions differed within and above the canopy. This may have led to diabatic flows controlled by changes in air density and the slope [60], which localized the source area for the storage flux. Thus, the influence of down-valley winds affecting the stability conditions, particularly at nighttime, existed. Interestingly, the transition time oscillated from underestimation during very unstable conditions to overestimation during stable conditions. The latter occurred due to advection above and within the forest canopy air space, which had also been observed by [32]. However, nighttime hours contributed the least to the EBC imbalance as u* and wind speeds declined while daytime, with high turbulence activities of u* up to 1.5 m/s and high wind speeds, generated a clear overestimation.

Another reason for the imbalance was the underestimation of G, which peaked during the late afternoon (14:00–15:00) as shown in Figure 4. This delay most likely developed due to the dense canopy of the tropical rainforest, which limited the absorption of SWin of the soil, which was also reflected in the soil temperature (Supplementary Materials,

Figures S1 and S2). The values varied between 15 to 16° C. The thermal wave propagation in the soil was delayed as the depth increased, meaning that temperature fluctuations at the surface took longer to affect deeper soil layers. The ground heat flux decreased with depth due to the insulating properties of the humus-rich layer, which is approximately 30 cm thick [70]. This effect is more pronounced under forested areas compared to grasslands [71].

The relationship between Rn and ϵ as functions of (z-d)/L and u^* showed that the highest net radiation gained the strongest overestimation as the atmosphere was weakly stable to neutral stratified (Figure 10). With a net radiation loss, imbalances weakened under stable conditions. With respect to turbulence activities, the strongest overestimations developed with increasing u^* values during the transition hours as indicated by the decreasing Rn values.

As biases in the energy fluxes resulted in biases in the carbon fluxes, the NEE was examined in the diurnal cycle and modelled with independent variables (Figures 11 and 12). The mean diurnal pattern in NEE revealed a clear underestimation compared to what was noted in [1,2]. This was likely due to underestimations during stable conditions. However, after filtering the fluxes, the magnitude of the carbon uptake was similar to what was noted in [38]. Modeling NEE revealed a good performance with $R^2 = 0.51$ and 0.49 for Rg and PPFD respectively, which underpins the quality of the carbon fluxes. Rg, in particular, plays a critical role in driving photosynthesis and carbon uptake, with peak values during less rainy months being $180-160 \, \text{W/m}^2$ under clear skies. During cloudy periods or diffuse light conditions, Rg was lower, generally ranging from 120 to $140 \, \text{W/m}^2$, but these conditions may still have promoted efficient carbon uptake.

5. Conclusions

Based on two years of EC measurements in the high Andean rainforest, the impact of the terrain and the vegetation height on the energy and carbon fluxes using the EBC and heat storage effect was examined. However, the EBC performance was good and in the range of previously reported measurements. The heat storage effect using S_H and S_{LE} improved the EBC although it was marginal. Based on the diurnal variations in the imbalances using ε , it could be stressed that during nighttime hours, the lack of the EBC was least. In fact, the strongest deviations occurred during the daytime and transition to morning hours when changing wind directions evolved, but with varying influences. While the daytime hours generated strong overestimations because of their very unstable conditions and increasing u* values associated with the north-eastern direction, the transition was rather characterized by both an overestimation during stable conditions and an underestimation during unstable conditions. The latter was particularly true during the transition to nighttime. Thus, diurnal variations in both the EBC and the heat storage should be considered, which is also relevant in coupled atmosphere–ecosystem modeling, when using EC measurements for comparison. The NEE was modeled using a non-linear light-response regression, which validated the accuracy of the flux measurements in this challenging environment. Our next steps will be the partitioning of the NEE in order to quantify the carbon sink function of the tropical mountain rainforest. This is also highly important as a basis for validations of ecological models.

Supplementary Materials: The following supporting information can be downloaded at: https://www.mdpi.com/article/10.3390/f15101828/s1, Figure S1. Representing monthly averages of global radiation (bar, W/m²) and air temperature (line, °C) for the entire measurement period; Figure S2. Representing monthly averages of soil moisture (bar, %) and soil temperature (line, °C) for the entire measurement period.

Author Contributions: Conceptualization, data evaluation and visualization, and writing the original draft, C.M. and K.T.; methodology, M.S.; funding acquisition, J.B. and K.T.; writing—review and editing, F.P.-C.; writing—review and editing, G.C.-R.; writing—review and editing, J.H.; writing—review and editing, O.L.; writing—review and editing, A.F. All authors have read and agreed to the published version of the manuscript.

Funding: This research was kindly funded by the German Research Foundation DFG in the scope of the DFG research unit FOR2730 "RESPECT" in the subproject A1 (BE1780/51-2, TR1201/3-2).

Data Availability Statement: Data are available on request (katja.trachte@b-tu.de).

Acknowledgments: The authors would like to thank the Ministerio del Ambiente, Agua y Transición Ecológica (MAATE) and the Instituto Nacional de Biodiversidad de Ecuador (INABIO) for granting research permits and the foundation "Nature and Culture International" (NCI) for providing research facilities.

Conflicts of Interest: The authors declare no conflicts of interest.

References

- 1. Malhi, Y.; Nobre, A.D.; Grace, J.; Kruijt, B.; Pereira, M.G.P.; Culf, A.; Scott, S. Carbon Dioxide Transfer over a Central Amazonian Rain Forest. *J. Geophys. Res.* **1998**, *103*, 31593–31612. [CrossRef]
- 2. Kosugi, Y.; Takanashi, S.; Ohkubo, S.; Matsuo, N.; Tani, M.; Mitani, T.; Tsutsumi, D.; Nik, A.R. CO₂ Exchange of a Tropical Rainforest at Pasoh in Peninsular Malaysia. *Agric. For. Meteorol.* **2008**, *148*, 439–452. [CrossRef]
- Tóta, J.; Roy Fitzjarrald, D.; Da Silva Dias, M.A.F. Amazon Rainforest Exchange of Carbon and Subcanopy Air Flow: Manaus LBA Site—A Complex Terrain Condition. Sci. World J. 2012, 2012, 165067. [CrossRef] [PubMed]
- 4. Tóta, J.; Fitzjarrald, D.R.; Staebler, R.M.; Sakai, R.K.; Moraes, O.M.M.; Acevedo, O.C.; Wofsy, S.C.; Manzi, A.O. Amazon Rain Forest Subcanopy Flow and the Carbon Budget: Santarém LBA-ECO Site. *J. Geophys. Res.* **2008**, *113*, 2007JG000597. [CrossRef]
- 5. Botía, S.; Komiya, S.; Marshall, J.; Koch, T.; Gałkowski, M.; Lavric, J.; Gomes-Alves, E.; Walter, D.; Fisch, G.; Pinho, D.M.; et al. The CO₂ Record at the Amazon Tall Tower Observatory: A New Opportunity to Study Processes on Seasonal and Inter-annual Scales. *Glob. Chang. Biol.* **2022**, *28*, 588–611. [CrossRef]
- 6. Hutyra, L.R.; Munger, J.W.; Saleska, S.R.; Gottlieb, E.; Daube, B.C.; Dunn, A.L.; Amaral, D.F.; De Camargo, P.B.; Wofsy, S.C. Seasonal Controls on the Exchange of Carbon and Water in an Amazonian Rain Forest. *J. Geophys. Res.* **2007**, *112*, 2006JG000365. [CrossRef]
- 7. Tan, Z.; Zhang, Y.; Yu, G.; Sha, L.; Tang, J.; Deng, X.; Song, Q. Carbon Balance of a Primary Tropical Seasonal Rain Forest. *J. Geophys. Res.* **2010**, *115*, 2009JD012913. [CrossRef]
- 8. Miller, S.D.; Goulden, M.L.; Menton, M.C.; Da Rocha, H.R.; De Freitas, H.C.; Figueira, A.M.E.S.; Dias De Sousa, C.A. Biometric and micrometeorological measurements of tropical forest carbon balance. *Ecol. Appl.* **2004**, *14*, 114–126. [CrossRef]
- 9. Kunert, N.; Aparecido, L.M.T. Ecosystem Carbon Fluxes Are Tree Size-Dependent in an Amazonian Old-Growth Forest. *Agric. For. Meteorol.* **2024**, *346*, 109895. [CrossRef]
- 10. Banbury Morgan, R.; Herrmann, V.; Kunert, N.; Bond-Lamberty, B.; Muller-Landau, H.C.; Anderson-Teixeira, K.J. Global Patterns of Forest Autotrophic Carbon Fluxes. *Glob. Chang. Biol.* **2021**, 27, 2840–2855. [CrossRef]
- 11. Costa, G.B.; Santos E Silva, C.M.; Mendes, K.R.; Dos Santos, J.G.M.; Neves, T.T.A.T.; Silva, A.S.; Rodrigues, T.R.; Silva, J.B.; Dalmagro, H.J.; Mutti, P.R.; et al. WUE and CO₂ Estimations by Eddy Covariance and Remote Sensing in Different Tropical Biomes. *Remote Sens.* **2022**, *14*, 3241. [CrossRef]
- Duque, A.; Peña, M.A.; Cuesta, F.; González-Caro, S.; Kennedy, P.; Phillips, O.L.; Calderón-Loor, M.; Blundo, C.; Carilla, J.; Cayola, L.; et al. Mature Andean Forests as Globally Important Carbon Sinks and Future Carbon Refuges. Nat. Commun. 2021, 12, 2138. [CrossRef] [PubMed]
- González-Jaramillo, V.; Fries, A.; Rollenbeck, R.; Paladines, J.; Oñate-Valdivieso, F.; Bendix, J. Assessment of Deforestation during the Last Decades in Ecuador Using NOAA-AVHRR Satellite Data. Erdkunde 2016, 70, 217–235. [CrossRef]
- 14. Curatola Fernández, G.; Obermeier, W.; Gerique, A.; López Sandoval, M.; Lehnert, L.; Thies, B.; Bendix, J. Land Cover Change in the Andes of Southern Ecuador—Patterns and Drivers. *Remote Sens.* 2015, 7, 2509–2542. [CrossRef]
- 15. Wright, S.J. Tropical Forests in a Changing Environment. Trends Ecol. Evol. 2005, 20, 553–560. [CrossRef]
- 16. Baldocchi, D.D. Assessing the Eddy Covariance Technique for Evaluating Carbon Dioxide Exchange Rates of Ecosystems: Past, Present and Future. *Glob. Chang. Biol.* **2003**, *9*, 479–492. [CrossRef]
- 17. Eddy Covariance: A Practical Guide to Measurement and Data Analysis; Aubinet, M.; Vesala, T.; Papale, D. (Eds.) Springer: Dordrecht, The Netherlands, 2012; ISBN 978-94-007-2350-4.
- 18. Papale, D.; Reichstein, M.; Aubinet, M.; Canfora, E.; Bernhofer, C.; Kutsch, W.; Longdoz, B.; Rambal, S.; Valentini, R.; Vesala, T.; et al. Towards a Standardized Processing of Net Ecosystem Exchange Measured with Eddy Covariance Technique: Algorithms and Uncertainty Estimation. *Biogeosciences* **2006**, *3*, 571–583. [CrossRef]
- 19. Foken, T.; Gockede, M.; Mauder, M.; Mahrt, L.; Amiro, B.; Munger, W. Post-Field Data Quality Control. In *Handbook of Micrometeorology*; Springer: Dordrecht, The Netherlands, 2004.
- 20. Trachte, K.; Bendix, J. Katabatic Flows and Their Relation to the Formation of Convective Clouds—Idealized Case Studies. *J. Appl. Meteorol. Climatol.* **2012**, *51*, 1531–1546. [CrossRef]
- 21. Trachte, K.; Nauss, T.; Bendix, J. The Impact of Different Terrain Configurations on the Formation and Dynamics of Katabatic Flows: Idealised Case Studies. *Bound. Layer Meteorol.* **2010**, *134*, 307–325. [CrossRef]

22. Foken, T.; Leuning, R.; Oncley, S.R.; Mauder, M.; Aubinet, M. Corrections and Data Quality Control. In *Eddy Covariance*; Aubinet, M., Vesala, T., Papale, D., Eds.; Springer: Dordrecht, The Netherlands, 2012; pp. 85–131. ISBN 978-94-007-2350-4.

- Mauder, M.; Foken, T.; Cuxart, J. Surface-Energy-Balance Closure over Land: A Review. Bound. Layer Meteorol. 2020, 177, 395

 –426.

 [CrossRef]
- 24. Kanda, M.; Inagaki, A.; Letzel, M.O.; Raasch, S.; Watanabe, T. LES Study of the Energy Imbalance Problem with Eddy Covariance Fluxes. *Bound. Layer Meteorol.* **2004**, *110*, 381–404. [CrossRef]
- 25. Novick, K.A.; Oishi, A.C.; Miniat, C.F. Cold Air Drainage Flows Subsidize Montane Valley Ecosystem Productivity. *Glob. Chang. Biol.* **2016**, 22, 4014–4027. [CrossRef] [PubMed]
- 26. Mammarella, I.; Kolari, P.; Rinne, J.; Keronen, P.; Pumpanen, J.; Vesala, T. Determining the Contribution of Vertical Advection to the Net Ecosystem Exchange at Hyytiälä Forest, Finland. *Tellus B Chem. Phys. Meteorol.* **2007**, *59*, 900. [CrossRef]
- 27. Turnipseed, A.A.; Blanken, P.D.; Anderson, D.E.; Monson, R.K. Energy Budget above a High-Elevation Subalpine Forest in Complex Topography. *Agric. For. Meteorol.* **2002**, *110*, 177–201. [CrossRef]
- 28. Novick, K.; Brantley, S.; Miniat, C.F.; Walker, J.; Vose, J.M. Inferring the Contribution of Advection to Total Ecosystem Scalar Fluxes over a Tall Forest in Complex Terrain. *Agric. For. Meteorol.* **2014**, *185*, 1–13. [CrossRef]
- 29. Baldocchi, D.D. How Eddy Covariance Flux Measurements Have Contributed to Our Understanding of *Global Change Biology*. *Glob. Chang. Biol.* **2020**, 26, 242–260. [CrossRef]
- 30. Wang, T.; Alfieri, J.; Mallick, K.; Arias-Ortiz, A.; Anderson, M.; Fisher, J.B.; Girotto, M.; Szutu, D.; Verfaillie, J.; Baldocchi, D. How Advection Affects the Surface Energy Balance and Its Closure at an Irrigated Alfalfa Field. *Agric. For. Meteorol.* **2024**, 357, 110196. [CrossRef]
- 31. Cuxart, J.; Wrenger, B.; Martínez-Villagrasa, D.; Reuder, J.; Jonassen, M.O.; Jiménez, M.A.; Lothon, M.; Lohou, F.; Hartogensis, O.; Dünnermann, J.; et al. Estimation of the Advection Effects Induced by Surface Heterogeneities in the Surface Energy Budget. *Atmos. Chem. Phys.* **2016**, *16*, 9489–9504. [CrossRef]
- 32. McGloin, R.; Šigut, L.; Havránková, K.; Dušek, J.; Pavelka, M.; Sedlák, P. Energy Balance Closure at a Variety of Ecosystems in Central Europe with Contrasting Topographies. *Agric. For. Meteorol.* **2018**, 248, 418–431. [CrossRef]
- 33. Gao, Z.; Liu, H.; Katul, G.G.; Foken, T. Non-Closure of the Surface Energy Balance Explained by Phase Difference between Vertical Velocity and Scalars of Large Atmospheric Eddies. *Environ. Res. Lett.* **2017**, 12, 034025. [CrossRef]
- Moderow, U.; Aubinet, M.; Feigenwinter, C.; Kolle, O.; Lindroth, A.; Mölder, M.; Montagnani, L.; Rebmann, C.; Bernhofer, C. Available Energy and Energy Balance Closure at Four Coniferous Forest Sites across Europe. *Theor. Appl. Clim.* 2009, 98, 397–412.
 [CrossRef]
- 35. Lindroth, A.; Mölder, M.; Lagergren, F. Heat Storage in Forest Biomass Improves Energy Balance Closure. *Biogeosciences* **2010**, 7, 301–313. [CrossRef]
- Swenson, S.C.; Burns, S.P.; Lawrence, D.M. The Impact of Biomass Heat Storage on the Canopy Energy Balance and Atmospheric Stability in the Community Land Model. J. Adv. Model Earth Syst. 2019, 11, 83–98. [CrossRef]
- 37. Meier, R.; Davin, E.L.; Swenson, S.C.; Lawrence, D.M.; Schwaab, J. Biomass Heat Storage Dampens Diurnal Temperature Variations in Forests. *Environ. Res. Lett.* **2019**, *14*, 084026. [CrossRef]
- 38. Hammerle, A.; Haslwanter, A.; Schmitt, M.; Bahn, M.; Tappeiner, U.; Cernusca, A.; Wohlfahrt, G. Eddy Covariance Measurements of Carbon Dioxide, Latent and Sensible Energy Fluxes above a Meadow on a Mountain Slope. *Bound. Layer Meteorol.* **2007**, 122, 397–416. [CrossRef]
- 39. Hiller, R.; Zeeman, M.J.; Eugster, W. Eddy-Covariance Flux Measurements in the Complex Terrain of an Alpine Valley in Switzerland. *Bound. Layer Meteorol.* **2008**, 127, 449–467. [CrossRef]
- 40. Del Castillo, E.G.; Paw U, K.T.; Sánchez-Azofeifa, A. Turbulence Scales for Eddy Covariance Quality Control over a Tropical Dry Forest in Complex Terrain. *Agric. For. Meteorol.* **2018**, 249, 390–406. [CrossRef]
- 41. Turnipseed, A.A.; Anderson, D.E.; Burns, S.; Blanken, P.D.; Monson, R.K. Airflows and Turbulent Flux Measurements in Mountainous Terrain. *Agric. For. Meteorol.* **2004**, *125*, 187–205. [CrossRef]
- 42. Callañaupa Gutierrez, S.; Segura Cajachagua, H.; Saavedra Huanca, M.; Flores Rojas, J.; Silva Vidal, Y.; Cuxart, J. Seasonal Variability of Daily Evapotranspiration and Energy Fluxes in the Central Andes of Peru Using Eddy Covariance Techniques and Empirical Methods. *Atmos. Res.* **2021**, 261, 105760. [CrossRef]
- 43. Homeier, J.; Werner, F.A.; Gradstein, S.R.; Breckle, S.W.; Richter, M. Potential vegetation and floristic composition of Andean forests in south Ecuador, with a focus on the RBSF. In *Gradients in a Tropical Mountain Ecosystem of Ecuador*; Beck, E., Bendix, J., Kottke, I., Makeschin, F., Mosandl, R., Eds.; Springer: Berlin/Heidelberg, Germany, 2008; Volume 221, pp. 87–100.
- 44. Chave, J.; Réjou-Méchain, M.; Búrquez, A.; Chidumayo, E.; Colgan, M.S.; Delitti, W.B.C.; Duque, A.; Eid, T.; Fearnside, P.M.; Goodman, R.C.; et al. Improved Allometric Models to Estimate the Aboveground Biomass of Tropical Trees. *Glob. Chang. Biol.* **2014**, *20*, 3177–3190. [CrossRef]
- 45. Trachte, K. Atmospheric Moisture Pathways to the Highlands of the Tropical Andes: Analyzing the Effects of Spectral Nudging on Different Driving Fields for Regional Climate Modeling. *Atmosphere* **2018**, *9*, 456. [CrossRef]
- 46. Raffelsbauer, V.; Pucha-Cofrep, F.; Strobl, S.; Knüsting, J.; Schorsch, M.; Trachte, K.; Scheibe, R.; Bräuning, A.; Windhorst, D.; Bendix, J.; et al. Trees with Anisohydric Behavior as Main Drivers of Nocturnal Evapotranspiration in a Tropical Mountain Rainforest. *PLoS ONE* 2023, 18, e0282397. [CrossRef] [PubMed]

47. Wilcke, W.; Yasin, S.; Schmitt, A.; Valarezo, C.; Zech, W. Soils Along the Altitudinal Transect and in Catchments. In *Gradients in a Tropical Mountain Ecosystem of Ecuador*; Beck, E., Bendix, J., Kottke, I., Makeschin, F., Mosandl, R., Eds.; Ecological Studies; Springer: Berlin/Heidelberg, Germany, 2008; Volume 198, pp. 75–85, ISBN 978-3-540-73525-0.

- 48. Finkelstein, P.L.; Sims, P.F. Sampling Error in Eddy Correlation Flux Measurements. *J. Geophys. Res.* **2001**, *106*, 3503–3509. [CrossRef]
- 49. Mauder, M.; Cuntz, M.; Drüe, C.; Graf, A.; Rebmann, C.; Schmid, H.P.; Schmidt, M.; Steinbrecher, R. A Strategy for Quality and Uncertainty Assessment of Long-Term Eddy-Covariance Measurements. *Agric. For. Meteorol.* **2013**, *169*, 122–135. [CrossRef]
- 50. Moncrieff, J.B.; Massheder, J.M.; De Bruin, H.; Elbers, J.; Friborg, T.; Heusinkveld, B.; Kabat, P.; Scott, S.; Soegaard, H.; Verhoef, A. A System to Measure Surface Fluxes of Momentum, Sensible Heat, Water Vapour and Carbon Dioxide. *J. Hydrol.* 1997, 188–189, 589–611. [CrossRef]
- 51. Eddy Covariance Method: For Scientific, Regulatory, and Commercial Applications; Updated and Expanded 2022 Edition; LI-COR Biosciences: Lincoln, NE, USA, 2022; ISBN 978-0-578-97714-0.
- 52. Webb, E.K.; Pearman, G.I.; Leuning, R. Correction of Flux Measurements for Density Effects Due to Heat and Water Vapour Transfer. *Quart. J. R. Meteoro. Soc.* **1980**, *106*, 85–100. [CrossRef]
- 53. Wilczak, J.M.; Oncley, S.P.; Stage, S.A. Sonic Anemometer Tilt Correction Algorithms. *Bound. Layer Meteorol.* **2001**, 99, 127–150. [CrossRef]
- 54. Kljun, N.; Calanca, P.; Rotach, M.W.; Schmid, H.P. A Simple Parameterisation for Flux Footprint Predictions. *Bound. Layer Meteorol.* **2004**, *1*12, 503–523. [CrossRef]
- 55. Barr, A.G.; Richardson, A.D.; Hollinger, D.Y.; Papale, D.; Arain, M.A.; Black, T.A.; Bohrer, G.; Dragoni, D.; Fischer, M.L.; Gu, L.; et al. Use of Change-Point Detection for Friction–Velocity Threshold Evaluation in Eddy-Covariance Studies. *Agric. For. Meteorol.* **2013**, 171–172, 31–45. [CrossRef]
- 56. Leuning, R.; Van Gorsel, E.; Massman, W.J.; Isaac, P.R. Reflections on the Surface Energy Imbalance Problem. *Agric. For. Meteorol.* **2012**, *156*, 65–74. [CrossRef]
- 57. Olmo, F.J.; Vida, J.; Foyo, I.; Castro-Diez, Y.; Alados-Arboledas, L. Prediction of Global Irradiance on Inclined Surfaces from Horizontal Global Irradiance. *Energy* **1999**, 24, 689–704. [CrossRef]
- 58. Bendix, J.; Aguire, N.; Beck, E.; Bräuning, A.; Brandl, R.; Breuer, L.; Böhning-Gaese, K.; De Paula, M.D.; Hickler, T.; Homeier, J.; et al. A Research Framework for Projecting Ecosystem Change in Highly Diverse Tropical Mountain Ecosystems. *Oecologia* **2021**, 195, 589–600. [CrossRef] [PubMed]
- 59. Meeus, J.A. Astronomical Algorithms, 2nd ed.; Willmann-Bell Inc.: Richmond, VA, USA, 1998.
- 60. Nicolini, G.; Aubinet, M.; Feigenwinter, C.; Heinesch, B.; Lindroth, A.; Mamadou, O.; Moderow, U.; Mölder, M.; Montagnani, L.; Rebmann, C.; et al. Impact of CO₂ Storage Flux Sampling Uncertainty on Net Ecosystem Exchange Measured by Eddy Covariance. *Agric. For. Meteorol.* **2018**, 248, 228–239. [CrossRef]
- 61. Finnigan, J. The Storage Term in Eddy Flux Calculations. Agric. For. Meteorol. 2006, 136, 108–113. [CrossRef]
- 62. Sakai, R.K.; Fitzjarrald, D.R.; Moore, K.E. Importance of Low-Frequency Contributions to Eddy Fluxes Observed over Rough Surfaces. *J. Appl. Meteor.* **2001**, *40*, 2178–2192. [CrossRef]
- 63. Stoy, P.C.; Mauder, M.; Foken, T.; Marcolla, B.; Boegh, E.; Ibrom, A.; Arain, M.A.; Arneth, A.; Aurela, M.; Bernhofer, C.; et al. A Data-Driven Analysis of Energy Balance Closure across FLUXNET Research Sites: The Role of Landscape Scale Heterogeneity. *Agric. For. Meteorol.* 2013, 171–172, 137–152. [CrossRef]
- 64. Twine, T.E.; Kustas, W.P.; Norman, J.M.; Cook, D.R.; Houser, P.R.; Meyers, T.P.; Prueger, J.H.; Starks, P.J.; Wesely, M.L. Correcting Eddy-Covariance Flux Underestimates over a Grassland. *Agric. For. Meteorol.* **2000**, *103*, 279–300. [CrossRef]
- 65. Matthews, B.; Mayer, M.; Katzensteiner, K.; Godbold, D.L.; Schume, H. Turbulent Energy and Carbon Dioxide Exchange along an Early-successional Windthrow Chronosequence in the European Alps. *Agric. For. Meteorol.* **2017**, 232, 576–594. [CrossRef]
- 66. Tan, Z.-H.; Zhang, Y.-P.; Schaefer, D.; Yu, G.-R.; Liang, N.; Song, Q.-H. An Old-Growth Subtropical Asian Evergreen Forest as a Large Carbon Sink. *Atmos. Environ.* **2011**, 45, 1548–1554. [CrossRef]
- 67. Sullivan, M.J.P.; Talbot, J.; Lewis, S.L.; Phillips, O.L.; Qie, L.; Begne, S.K.; Chave, J.; Cuni-Sanchez, A.; Hubau, W.; Lopez-Gonzalez, G.; et al. Diversity and Carbon Storage across the Tropical Forest Biome. *Sci. Rep.* **2017**, *7*, 39102. [CrossRef]
- 68. Franssen, H.J.H.; Stöckli, R.; Lehner, I.; Rotenberg, E.; Seneviratne, S.I. Energy Balance Closure of Eddy-Covariance Data: A Multisite Analysis for European FLUXNET Stations. *Agric. For. Meteorol.* **2010**, *150*, 1553–1567. [CrossRef]
- 69. Loescher, H.W.; Law, B.E.; Mahrt, L.; Hollinger, D.Y.; Campbell, J.; Wofsy, S.C. Uncertainties in, and Interpretation of, Carbon Flux Estimates Using the Eddy Covariance Technique. *J. Geophys. Res.* **2006**, *111*, 2005JD006932. [CrossRef]
- 70. Velescu, A.; Valarezo, C.; Wilcke, W. Response of Dissolved Carbon and Nitrogen Concentrations to Moderate Nutrient Additions in a Tropical Montane Forest of South Ecuador. *Front. Earth Sci.* **2016**, *4*, 58. [CrossRef]
- 71. Bendix, J.; Rafiqpoor, D.M. Studies on the Thermal Conditions of Soils at the Upper Tree Line in the Páramo of Papallacta (Eastern Cordillera of Ecuador). *Erdkunde* **2001**, *55*, 257–276. [CrossRef]

Disclaimer/Publisher's Note: The statements, opinions and data contained in all publications are solely those of the individual author(s) and contributor(s) and not of MDPI and/or the editor(s). MDPI and/or the editor(s) disclaim responsibility for any injury to people or property resulting from any ideas, methods, instructions or products referred to in the content.